Materials Science and Engineering B 263 (2021) 114807

Contents lists available at ScienceDirect

Materials Science & Engineering B

journal homepage: www.elsevier.com/locate/mseb

Optimisation of the green synthesis of Cu/Cu_2O particles for maximum yield production and reduced oxidation for electronic applications

Sandra Sampaio *, Júlio C. Viana

IPC – Institute of Polymers and Composites, University of Minho, Campus de Azurem, 4804-533 Guimarães, Portugal

ARTICLE INFO

Keywords:
Copper microparticles/nanoparticles
Green synthesis
Taguchi method
Cu/Cu_2O phases
Electrical resistivity

ABSTRACT

Taguchi method with an L8 orthogonal array and analysis of variance (ANOVA) were used to evaluate the effect of pH, amount of *Cynara scolymus L.*(artichoke) extract (AE), copper salt concentration (SC) and temperature (T) on the optimization of green synthesis of copper microparticles with respect to the maximization of the yield production and, for the first time, with respect to the minimization of the oxidation degree of the copper microparticles. Results indicate that pH and AE have greater influence on the Cu/Cu_2O microparticles yield. While the pH, AE and T have greater influence on the oxidation degree of the Cu/Cu_2O microparticles. XRD confirmed the minimization of Cu_2O phase over Cu/Cu_2O mixture, reducing Cu_2O from 83% to 31%. Spherical particles of 324–711 nm were observed and the electrical resistivity of Cu/Cu_2O (69/31 wt%) was 1.52×10^{-3} Ω.cm.

1. Introduction

Copper particles in its metallic and oxidized forms have attracted increased attention because they are widely used in various fields based on their unique magnetic, electronic, optical, catalytic, antifungal and antibacterial properties along with their low cost [1]. They are used in conductive inks [2], batteries [3,4], solar cells [5], biosensing [6], gas sensing [7], electrochemical sensing [8], catalysis [9,10], water treatment [11], bactericidal agent [12], antimicrobial agent [13], antifungal agent [14] and anticancer agent [15]. Currently, conductive inks using copper nanoparticles are investigated for application in the growing printed electronics market, for example, printed circuit boards, light emitting devices, radio frequency identification antenas (RFIDs) and thin film transistors, due to its high conductivity and lower cost [16]. However copper nanoparticles has an inherent tendency to oxidize in aqueous synthesis conditions and can reduce its electrical conductivity. Thus the prevention of copper oxidation is crucial to prepare conductive inks [17]. In the past decade researchers have demonstrated that copper particles' properties are strongly influenced by the shape, size and oxidation state of the Cu nanocrystals. This has invigorated an upsurge in research on new synthesis routes of copper particles [18]. There are different methods of synthesis of copper nanoparticles including: polyol process, metal vapour synthesis, laser ablation, micro-emulsion techniques, chemical reduction, thermal reduction and in situ chemical synthesis [19]. However, these production methods are usually expensive, labour-intensive, and are potentially hazardous to the environment and living organisms [20]. Thus, there is a demand for alternative processes that guarantee clean, non-toxic, environmentally friendly and cost-effective methods to produce copper particles. In recent years, it has been demonstrated that many biological systems, including plants [21,22] and algae [23], diatoms [24], bacteria [25], yeast [26], fungi [27], and human cells [28], emerged as green alternatives of synthesis of nanoparticles. The green synthesis of particles using plants displays important advantages over other biological systems, such as low cost of cultivation, the ability to up production volumes and it is simpler, quicker and safer. Following this route, Cu particles in its metallic and oxide forms have been synthesized in aqueous media by a variety of plant extracts: magnolia leaf [29], Punica granatum [30], Hibicus rosasinensis [31], Eclipta prostrata [32], Capparis zeylanica [33] and Gloriosa superba L [34] . These plants were reported to have biomolecules, including carbohydrates, proteins and phenolic compounds, which are used in the reduction and capping of copper ions to form nano or microparticles. In spite of the fact that these research works used green synthesis for production of copper particles with the several advantages such as the environmentally friendliness of the process and more biocompatible final products, the optimization of process parameters has been less explored, together with the less assessment of their electrical properties (as relevant for obtaining conductive inks).

The source of the plant extract (their active biomolecules types and

* Corresponding author.
E-mail address: sandramonteirosampaio@gmail.com (S. Sampaio).

https://doi.org/10.1016/j.mseb.2020.114807
Received 14 April 2020; Received in revised form 12 June 2020; Accepted 14 September 2020
Available online 25 September 2020

concentration) plays a major role in influencing the shape, size, yield and surface properties of nanoparticles [35]. Artichoke (*Cynara scolymus L.*) plant is a rich source of polyphenolic compounds, with cynarin, a caffeoylquinic acid derivative, being the most well know compound. Other phenolics such as flavones, apigenin and luteolin, and anthocyanidinscyanidin, peonidin and delphinidin have also been found. It has been reported that the phenolic compounds of artichoke extracts are responsible for antioxidant activity, the polyphenols being able to reduce the abnormally increased levels of reactive oxygen species (ROS) that were found in a wide range of disorders, including inflammatory bowel disease and cancer [36]. Due to artichoke's low cost and its environmental-friendly nature along with its antioxidant properties, artichoke (*Cynara scolymus L.*) was selected as reducing and capping agent to prepare copper particles in our work. In spite of its nutritional and pharmaceutical applications, the wastes originated by the industry (e.g. canning industry) are high, constituting c.a. 80%–85% of the total biomass of the plant [37]. In 2016, the global production of artichoke almost reached 1.5 MTon [38]. The potential of *Cynara scolymus L.* (CS) for green synthesis of copper particles is therefore huge. The use of *CS* extract for green synthesis of copper microparticles has not been reported yet. Recently *Cynara scolymus L.* flower extract has been used in the synthesis of silver nanoparticles [39].

Process optimization by design of experiments, such as the Taguchi method, provides a simple and effective approach that minimizes the number of experimental tests and resources, which reduces the time and the costs of experiments [40]. Compared to the full factorial method, instead of testing all possible combinations of the parameters available, Taguchi method provides a more simplified way to setup the combination of experimental parameters using orthogonal arrays [41]. Although the Taguchi method has been applied to the optimization of green synthesis of particles, including the green synthesis of silver particles and gold particles using plant extracts [42,43], the green synthesis of CuO particles using bacterial approach [44] and the green synthesis of silver particles using fungi extracts [45], the purpose of these studies was to screen the key parameters for the green synthesis of smaller sized particles or to maximize the yield of particles.

Hence, there is a need to select the key parameters for the green synthesis of Cu particles with reduced oxidation degree, in a reliable, cost-effective and environmentally friendly process, in order to obtain the higher electrical conductivity of the produced Cu particles. So far, no work has been reported in literature for the minimization of the oxidation state of Cu nanocrystals during their synthesis using Taguchi's experimental design methodology. In the present work, the Taguchi method with an L8 orthogonal array (4 variables, 2 levels, 8 tests) and analysis of variance (ANOVA) techniques were used to evaluate statistically the effect of pH, amount of CS extract (AE), copper salt concentration (SC) and temperature (T) on the optimization of the green synthesis of copper particles using flower extract of *Cynara scolymus L.* with respect to the maximization of the yield production of copper microparticles and to the minimization of the oxidation state of the copper microparticles during their synthesis. Then, the produced green copper microparticles particles were characterized by UV–Vis, XRD, SEM, EDS analysis and electrical resistivity measurements. Knowledge of the exact oxidation degree of the synthesized Cu particles and its effect on their electrical conductivity is essential from an application perspective, e.g. in conductive inks as required in the emergent printed electronics technology.

2. Materials and methods

2.1. Materials and extract preparation

Hydrated copper nitrate [$Cu(NO_3)_2{\cdot}3H_2O$] and sodium hydroxide were purchased from Sigma-Aldrich. Fresh artichoke (*Cynara scolymus L.*) flower heads were purchased from a local market (Braga, Portugal), and they were washed with running tap water, to remove impurities, and dried at air. For the preparation of the CS extract, 20 g of washed flower petals cut in small pieces were added to 100 mL boiled water for 15 min. The extract was cooled at room temperature, filtered and stored at 4℃ for further use.

2.2. Green synthesis of copper microparticles

The general procedure for the green synthesis of copper microparticles is described in the following. CS extract was used as a reducing and capping agent and $Cu(NO_3)_2{\cdot}3H_2O$ was used as the copper salt precursor. In a 20 mL beaker, a solution of 4 mL of CS extract was added and adjusted to pH = 12 with 0.1 M NaOH, and then to this solution was slowly added a solution of 2.5 mL of 60 mM of $Cu(NO_3)_2{\cdot}3H_2O$; the mixture solution being continuously stirred for 1 h at 80℃. During the reaction time the reduction of $Cu(NO_3)_2{\cdot}3H_2O$ to copper microparticles was visually observed by the colour of the solution changing gradually to green and finally to yellow-orange colour, as shown in the Fig. 1. After synthesis, the copper microparticles were centrifuged and washed with distilled water. Finally, they were dried under vacuum at 60 °C overnight.

2.3. Experimental design

An experimental design, based on a Taguchi orthogonal array (OA), was employed to the green synthesis of copper microparticles in order to identify the optimal synthesis conditions for reaction yield maximization and minimization of particles oxidation, whilst keeping a low number of laboratory experiments and resources. The following parameters, which have a high impact on copper microparticles production, were selected: pH, temperature (T), amount of CS extract (AE) and copper salt concentration (SC). These parameters were varied in two levels, as shown in Table 1. A L8 Taguchi OA (with 8 experiments) was used to study the effect of the four parameters in the synthesis of copper particles, as listed in the Table 2. The studied response was the intensity of the absorbance peak at 565 nm of the solution after each experiment. This absorbance peak at 565 nm (from the UV–Vis spectra of the solution) corresponds to the surface plasmon resonance phenomenon of copper in the non-oxidized form [19]. The maximization of the intensity of this absorbance peak leads to a high throughput of Cu phase particles. The peak absorbance intensity at 386 nm was also analysed, this peak corresponding to the surface plasmon resonance phenomenon of copper oxide (Cu_2O) particles [19].

2.4. Characterization of green-synthesized copper microparticles

Green synthesis of copper microparticles was confirmed by measuring the absorbance in UV–Vis spectra at a wavelength range between 200 and 800 nm, at a resolution of 1 nm (spectrophotometer UV-240 1 PC, Shimadzu), after diluting a small aliquot of the copper microparticles solution with CS aqueous extract (blanket sample). The size and morphology of copper microparticles were observed by scanning electron microscope SEM (Leica-Cambridge S360 scanning electron microscope and the NanoSEM-FEI Nova 200 (FEG/SEM)). The sample was prepared by placing copper microparticles in powder form on a double sided carbon tape and, subsequently, transferring it to the microscope operated at an accelerated voltage of 15 kV. The elemental composition was also analysed by an energy dispersive x-ray spectrometer (EDS, combined with SEM). The e-beam used in EDS measurements had a diameter that was larger than the particle diameter. Therefore, the elemental composition obtained reflected the composition of both particle and surroundings. The structure phase and crystallinity of copper microparticles were studied by X-ray diffraction, in a Rigaku D/ max 2500 V equipped with Cu-Kα radiation source. This equipment was operated at a voltage of 30 kV and a current of 40 mA, over a 2θ angle range of 20° to 80°. X-ray diffraction patterns were analysed with TOPAS 4 software. The electrical resistance

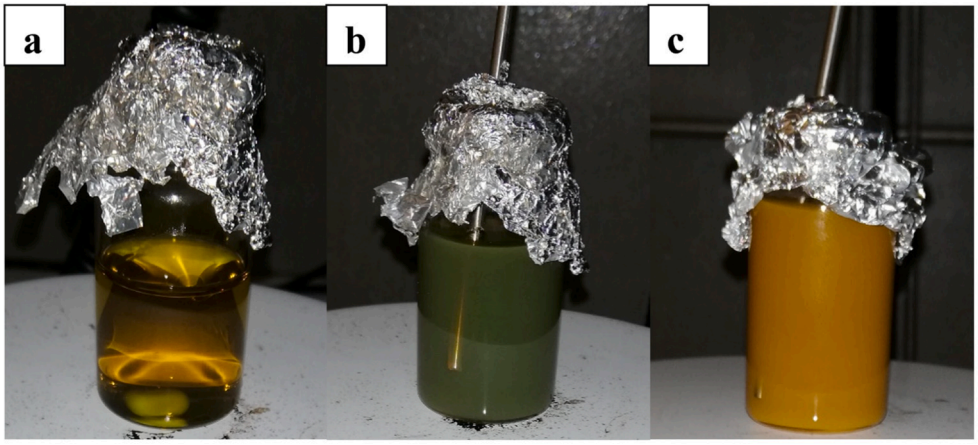

Fig. 1. Synthesis of copper microparticles using aqueous extract of *Cynara scolymus L.* (CS): (a) aqueous extract of CS; (b) aqueous extract of CS + $Cu(NO_3)_2{\cdot}3H_2O$ at 10 min reaction; (c) copper microparticles at 60 min reaction.

Table 1
Parameters and levels employed in the design of experiments.

Code	Parameter	Levels	
		1	2
A	pH	10	12
B	Amount of CS extract (mL), AE	4	5
C	Copper salt concentration (mM), SC	50	60
D	Temperature (C), T	80	90

Table 2
Taguchi Orthogonal Experimental Design (the runs were made randomly).

Run	pH	AE	SC	T	Absorbance at 565 nm	Absorbance at 386 nm
1	1	1	1	1	1.131	2.844
2	1	1	2	2	1.63	1.843
3	1	2	1	1	1.12	3.249
4	1	2	2	2	1.259	2.998
5	2	1	1	2	1.798	1.51
6	2	1	2	1	1.463	2.653
7	2	2	1	2	1.715	1.96
8	2	2	2	1	1.134	2.684

measurements were performed based on the Van der Pauw technique at ambient temperature. Powder discs (pressed into a circle of 1 cm^2 diameter, using a hydraulic press) were tested using a digital multimeter (Fluke 8846A) and in-house sample assembly jig with four flat ohmic contact probes of phosphor Bronze with 2.54 mmm diameter.

3. Results and discussions

3.1. UV–Vis spectra: Types of produced particles

Fig. 2 shows the UV–Vis spectra of the orthogonal array Table runs (Table 2). The variation of the synthesis parameters leads to the formation of Cu particles and/or its oxide with different amounts and sizes of particles. Three main groups of curves are observed:

a) curves with a small peak centred around 386 nm and a broad peak at 530–585 nm (Run 2, 5, and 7, having in common a high T setting);
b) curves with the highest peaks centred around 386 nm and a smaller peak at 465 nm (Run 1, 3, and 4, having in common a low pH value); and
c) curves with the highest peaks centred around 386 nm and a smaller peak at 500–530 nm (Run 6 and 8, only differentiated by the AE).

This indicates the formation of Cu particles and its oxide, with different amounts and size distributions, depending upon the used synthesis parameters. Generally, the position of the absorption peaks is related to the types of formed particles (e.g., Cu, CuO and Cu_2O) [19], the peak width to the size distribution, and the peak height to the number of produced particles. A high yield production of Cu particles can be obtained by increasing the height of the absorption peak at around 560–585 nm, by optimizing the synthesis parameters.

3.2. Optimization of the yield production green synthesis: Cu microparticles

In the Taguchi method, an orthogonal arrays and analysis of variance (ANOVA) tools are used for the experimental analysis. By using orthogonal arrays (OA) the minimum number of experiments is needed and by ANOVA the effect of the various parameters can be statistically estimated [46]. In this work, the interest was to maximize the yield production of Cu particles, so the height of the absorption peak at 565 nm (Table 2) is to be maximized.

Table 3 represents the ANOVA results for the height of this peak. The most significant main factors (with a 95% confidence level) are the pH, AE and T with a percentage of contribution of 20.9%, 14.4% and 8.3%, respectively. The SC variation does not affect the response. But there is a strong interaction between AE and SC, accounting for 54.3% of contribution. The high values of the coefficients of correlation, R^2 and adjusted-R^2, indicate that the selected model (considering the main factors: pH, AE, and T, and the interaction AE × SC) explains the total variation of 97.9% of the absorbance of the 565 nm peak, due to the chosen parameters variations. The model F-value of 35.01 implies that the selected model is significant with only of 0.75% of chance that such a high value could occur due to noise. From the p-values results, only the SC factor is not significant (with a confidence level of 95%). The following equation (coded factors) can be used for estimating the 565 nm peak height from the synthesis parameters:

$$Cu\ peak\ 565\ absorbance = 1.41 + 0.12pH + 0.10AE - 0.076T - 0.19AExSC \quad (1)$$

The parameters such as plant extract (types of phytochemicals, phytochemical concentration), metal salt concentration, pH, and temperature are admitted to control the rate of nanoparticle formation as well as their yield and stability [47]. In general, the mechanism of metallic nanoparticle formation by plant extract includes three phases: (1) the activation phase (reduction of metal ions/salts and nucleation process of the reduced metal ions), (2) the growth phase (spontaneous combination of tiny particles with greater ones) via a process

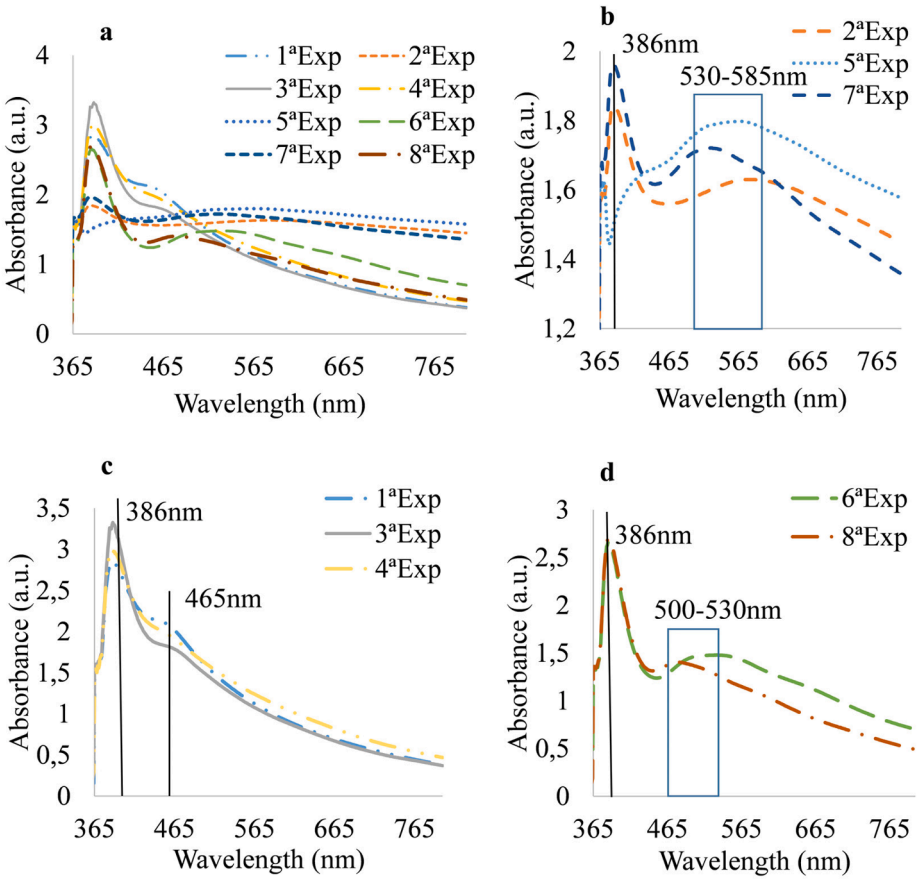

Fig. 2. (a) UV–Vis spectra of the produced microparticles (with parameters of Table 2); (b) UV–vis spectra of run 2, 5 and 7; (c) UV–vis spectra of run 1, 3 and 4; (d) UV–vis spectra of run 6 and 8.

Table 3
ANOVA results of the absorbance of 565 nm peak of the UV–Vis absorption spectra (Model – fitted linear model including significant factors and interactions; Residuals – or errors, is the difference between an observation and the model estimate; R2 (coefficient of determination); adjusted-R2 (modified form of R2 that has been adjusted by the number of factors in the model); SS – sum of squares; Df – degree of freedom; F-value – the F-statistic (F) from the mean square and its p-value; % of Contr.- % of contribution).

Sources	SS	Df	F-value	p-value	% of Contr.
Model	0.55	4	35.01	0.0075	–
pH	0.12	1	29.91	0.0120	20.9
Amount of Extract, AE	0.08	1	20.60	0.0200	14.4
Salt Content, SC	$1.458x10^{-3}$	–	0.29	0.6462	Not significant
Temperature, T	0.046	1	11.82	0.0412	8.3
AE × SC	0.30	1	77.72	0.0031	54.3
Residuals	0.010	3	–	–	2.1
R^2	0.9790	–	–	–	–
Adjusted R^2	0.9511	–	–	–	–

acknowledged as Ostwald ripening, and (3) the last one is termination phase (defining the final shape of the nanoparticles) [20]. Nonetheless, the exact fundamental mechanism for metal oxide nanoparticle preparation via plant extracts is still not fully understood [47 20]. Fig. 3 shows the variations of the 565 nm peak absorbance with the synthesis parameters. The peak absorbance increases with the increment of pH and AE. This change in pH results in an electric charge change on the natural biomolecules contained in the extract, which affects their ability to bind and reduce metal ions in the course of particles synthesis [48]. Thus, the formation of Cu phase might increase, and the peak absorbance intensity at 565 nm increases. Increasing AE results in a faster nucleation rate (owing to an enhanced reduction process) and higher number of particles are produced [20]. This peak absorbance decreases with the increment of T. According to the reaction temperature, nucleation or growth processes can be favoured [49]. In this case, an increase in temperature may favour the growth process, which in the course of particles synthesis, during the particles growth, new nuclei might aggregate around the already formed nuclei, forming large particles rather than new particles and consequently the peak absorbance intensity at 565 nm decreases. The interaction between AE and SC is strong. For low values of SC (SC1, i.e. 50 mM), the peak absorbance increases with AE. But for high values of SC (SC2, i.e. 60 mM), the peak absorbance decreases with AE. This increase on the peak absorbance for SC1 with increasing AE might be a result of an increment in the nucleation owing to the enhanced reduction process and, consequently, the particles production also increased. Distinctly for SC2, there is a decrease in the peak absorbance with increasing AE. Further increment upon AE (that also enhanced the reduction process) might result in further growth of the particles and, consequently, formed particles with larger diameters. The decrement of the maximum absorbance suggests the aggregation and precipitation of the particles.

Based on these results, the maximum value of 565 nm absorbance, which is related to a high production of Cu nanoparticles, could be achieved when the pH is 12, the amount of CS extract is 5 mL, the copper salt precursor is 50 mM and the temperature is 80°C.

3.3. Characterization of green synthesized copper microparticles with the highest yield production

A confirmation run with optimum parameter values above referred to was performed.

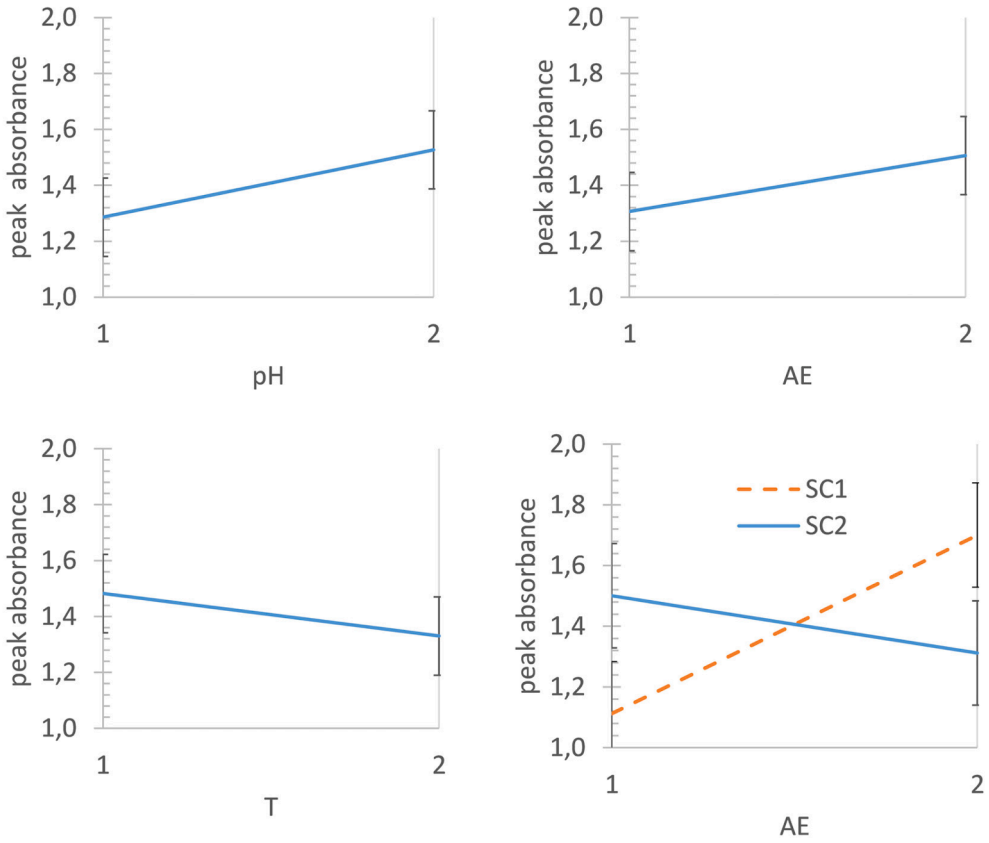

Fig. 3. Variation of the height of the absorbance of peak 565 nm with the synthesis parameters.

3.3.1. UV–Visible spectral analysis

Fig. 4 shows UV–Vis spectrum of the confirmation run. The two absorption bands due to the surface plasmon resonance (SPR) of Cu_2O and Cu particles are observed at 386 nm and at around 560–585 nm, respectively [19]. The broadness of the absorption peak at around 560–585 nm probably stems from a wide size distribution of particles. These observations suggest the existence of both copper oxide (Cu_2O) and copper (Cu) microparticles having size variations.

The value obtained for the absorbance at 565 nm of the confirmation run was 1.813, which is in good agreement with the predicted value with equation (1) of 1.897 (an error of 4.6%). This value is higher than the ones of Table 2, showing that the peak height was maximised (and hence the amount of Cu particles). The value is slight higher than the one obtained for run 5 (Table 2) of 1.798, with the following parameters: pH = 12, AE of 4 mL CS extract, 2.5 mL of 50 mM $Cu(NO_3)_2{\cdot}3H_2O$, and 90C for 1 h. Compared to confirmation run, the differences are the higher amount of extract, which has a significant contribution (14,4%) and the higher solution temperature, which was found to have a small percentage contribution (Table 3).

The highest yield production of confirmation run was also measured by the dry weight of microparticles. Under the optimum parameters a maximum of 4,5 mg/mL of Cu/Cu_2O microparticles was synthesized (confirmation run). This measurement is higher than the ones obtained for run 5 and run 7 (the highest values obtained for the absorbance at 565 nm in Table 2) of 4.3 mg/mL and 3.7 mg/mL respectively, confirming the optimization of the yield production of particles.

These results evidence that the amount of copper microparticles can be maximised. Nevertheless, a dual composition of Cu_2O and Cu particles was still obtained, with a narrow distribution of particles sizes of the former and a large size distribution of the latest.

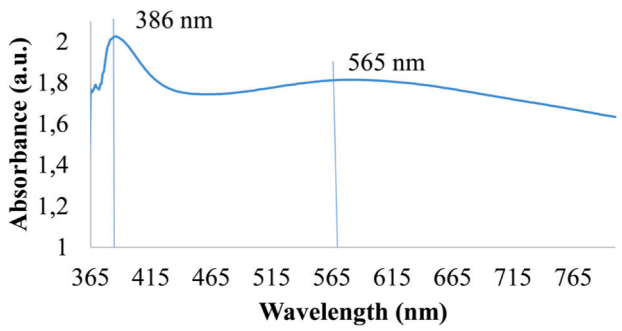

Fig. 4. UV–Vis absorption spectrum of microparticles produced using optimum synthesis parameters (confirmation run).

3.3.2. X-ray diffraction (XRD) analysis

XRD pattern of green synthesized copper microparticles from confirmation run is shown in Fig. 5. The XRD pattern shows a high crystallinity with diffraction peaks at 43.46°, 50.36° and 74.66°, which can be assigned respectively to (1 1 1), (2 0 0) and (2 2 0) crystal planes of face-centred cubic (fcc) of Cu particles (which is in good agreement with the Joint Committee on Powder Difraction Standards, JCPDS, file No. 040836) [50] and peaks at 29.87°, 36.47°, 42.77, 62.27° and 74.30°, which corresponds to the (1 1 0), (1 1 1), (2 0 0), (2 2 0), (3 1 1) diffraction planes of face-centered cubic (fcc) of Cu_2O particles, respectively (JCPDS No. 050667) [51]. This XRD pattern indicates the presence of mixed phases of copper (Cu) and copper oxide (Cu_2O), confirming the results obtained from UV–Vis analysis. Analysis of the ratio of Cu and Cu_2O determined from TOPAS software is 17% and 83%, respectively.

3.3.3. Energy dispersive x- ray spectroscopy (EDS) analysis

In addition, the elemental content of the produced microparticles was assessed using EDS analysis, as shown in Fig. 6. The microparticles are composed of Cu along with O and C elements. The presence of Cu,

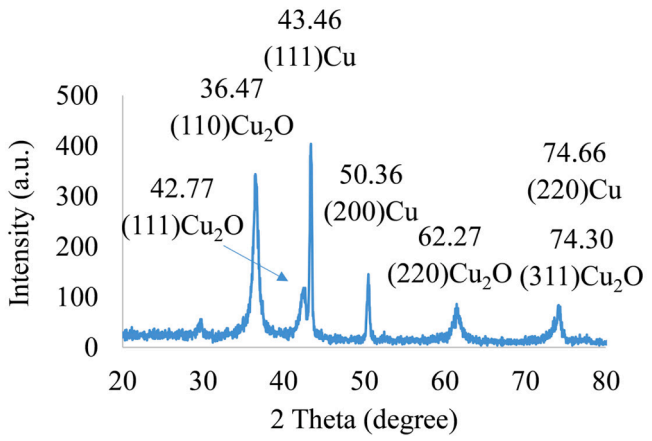

Fig. 5. XRD diffractogram of microparticles synthesized by CS extract using optimum synthesis parameters (confirmation run).

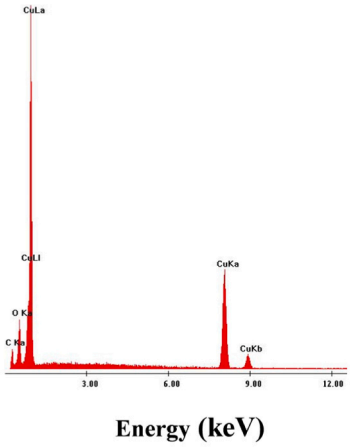

Fig. 6. EDS analysis of copper microparticles synthesized by CS extract using optimum synthesis parameters (confirmation run).

the main element, confirms the formation of Cu microparticles. The presence of O indicates that at least part of the copper microparticles are oxidized [52]. The presence of C possibly originates from the CS biomolecules attached to the surface of microparticles [39] and/or from the double sided carbon tape used for SEM grid preparation. The weight percent of copper (Cu), oxygen (O), and carbon (C) was found out to be of 73.8%, 13.6%, and 12.7%, respectively. Traces of other elements are not present reflecting the purity of the microparticles. The results indicated that the microparticles synthesized from CS extract by Taguchi optimized synthesis (confirmation run) are copper which might be in its metallic and oxidized forms.

3.3.4. Scanning electron microscopy (SEM) analysis

The size and surface morphology of the confirmation run was obtained by SEM analysis. Fig. 7 revealed the production of a high density of copper particles with spherical shape and particles sizes between 0.364 and 1.225 μm in diameter. SEM image proved the wide size distribution of microparticles, already observed in the UV–Vis spectra.

3.4. Optimization of copper phase (Cu) microparticles

The absorption peak at 386 nm corresponds to the presence of copper oxide (Cu_2O) microparticles [19]. Adopting a similar approach as for the case of highest throughput of Cu particles, the interest is now to minimize the production of Cu_2O particles, so the height of the absorption peak at 386 nm (Table 2) is to be minimized.

Table 4 presents the ANOVA results. The most significant factors (with a 95% confidence level) are the pH, AE and T with a percentage of 21.9%, 20.0% and 45.4%, respectively. The SC variation does not affect the response. The high values of the coefficients of correlation, R^2 and adjusted-R^2, indicate that the selected model (considering the main factors: pH, AE, and T) explains the total variation of 87.3% of the absorbance of the 386 nm peak, due to the chosen parameters variations. The model F-value of 9.13 implies that the selected model is significant with only of 2.91% of chance that such a high value could occur due to

Table 4
ANOVA results of the absorbance of 386 nm peak of the UV–Vis absorption spectra (Model – fitted linear model including significant factors and interactions; Residuals – or errors, is the difference between an observation and the model estimate; R2 (coefficient of determination); adjusted-R2 (modified form of R2 that has been adjusted by the number of factors in the model); SS – sum of squares; Df – degree of freedom; F-value – the F-statistic (F) from the mean square and its p-value; % of Contr.- % of contribution).

Sources	SS	Df	F-value	p-value	% of Contr.
Model	2.39	3	9.13	0.0291	–
pH	0.60	1	6.87	0.061	21.9
Amount of Extract, AE	0.55	1	6.27	0.057	20.0
Temperature, T	1.24	1	14.24	0.016	45.4
Residuals	0.349	4	–	–	12.7
R^2	0.8725	–	–	–	–
Adjusted R^2	0.7769	–	–	–	–

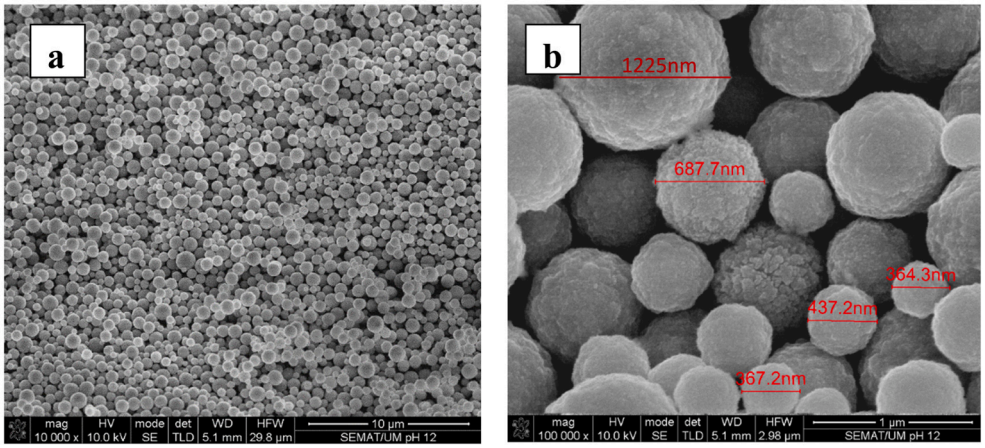

Fig. 7. (a, b) SEM image of copper microparticles synthesized by CS extract using optimum synthesis parameters (confirmation run), (b) displays the magnification of the microparticles.

noise. From the p-values results, only the SC factor (not shown in Table 4) is not significant (with a confidence level of 95%). The production of Cu_2O microparticles can be modelled by equation (2) (coded factors):

$$Cu\ peak\ 386\ absorbance = \quad 2.48 - 0.26pH + 0.26AE - 0.39\ T \tag{2}$$

Fig. 8 shows the variations of the 386 nm peak absorbance with the synthesis parameters. The peak absorbance decreases with the increment of pH and T. Due to changes in the pH, the electric charge present on the biomolecules of CS extract varies, which may influence their capping and stabilizing abilities [53] and hence the antioxidant ability of the particles. The antioxidant ability might be due to the biomolecules of CS extract present at the surface of particles (capping ability) having antioxidant activity [54]. Thus, the formation of Cu_2O phase might decrease, and the peak absorbance intensity at 386 nm decreases. This peak absorbance decreases with the increment of T. The temperature not only influences the reaction rate but also affects the stability of the colloidal solutions [49]. Increasing T may favour the stability of the resulting particles by increasing the interactions between particles and CS extract solution. These biomolecules pointing out from the metal surface and the resulting steric repulsion, might be the major mechanism for particles dispersion. This combination seems to form a protection against the growth rate of the oxidized shell on the particle, decreasing the Cu_2O particles formation. This peak absorbance increases with the increment of AE. This increase might be a result of an increment in the nucleation owing to the higher availability of reducing agent and, consequently, the particles production also increased.

Based on these results, the minimum value of 386 nm absorbance, which is related to a low production of Cu_2O microparticles, could be achieved when the pH is 12, the amount of CS extract is 4 mL, the copper salt precursor is 50 mM and the temperature is 90°C. This corresponds to run 5, which in fact showed the lowest value of the 368 nm peak (Table 2).

However, this set of synthesis parameters does not maximizes the production of Cu particles (obtained by the confirmation run).

It would be interesting to find the optimum reaction conditions that would obtain mostly Cu microparticles (pure Cu phase). The goal is now to determine the settings of synthesis parameters that simultaneously reduces the height of the 386 nm peak (Cu_2O particles) and increases the height of the 565 nm peak (Cu particles), i.e. maximize equation (1) and minimize equation (2) at the same time. This was done through a numerical optimization procedure, adopting a hill climbing technique, that searches for the best trade-offs between factors to achieve multiple goals through a desirability objective function[55]. The results of this simultaneous goals optimization resulted in the following set of parameters: pH equal to 12, the amount of CS extract of 5 mL, the copper salt precursor of 50 mM and the temperature of 90°C. This corresponds to run 7 (Table 2). This setting only differs from run 5 (minimization of 386 nm absorbance peak) by the higher adjustment of AE. Table 5 compares the settings of synthesis parameters for the different objectives of production of Cu microparticles. Common settings are the high setting of pH = 12 and low SC amount of 50 mM. The synthesized particles for each

Table 5
Synthesis parameters for different objectives of Cu microparticles production.

Objective:	pH	AE(mL CS extract)	SC(mM of Cu $(NO_3)_2{\cdot}3H_2O$)	T (°C)	Run
Max peak 565 (Cu NP)	12	5	50	80	Confirmation run
Min peak 386 (Cu_2O NP)	12	4	50	90	5
Max 565 and Min peak 386	12	5	50	90	7

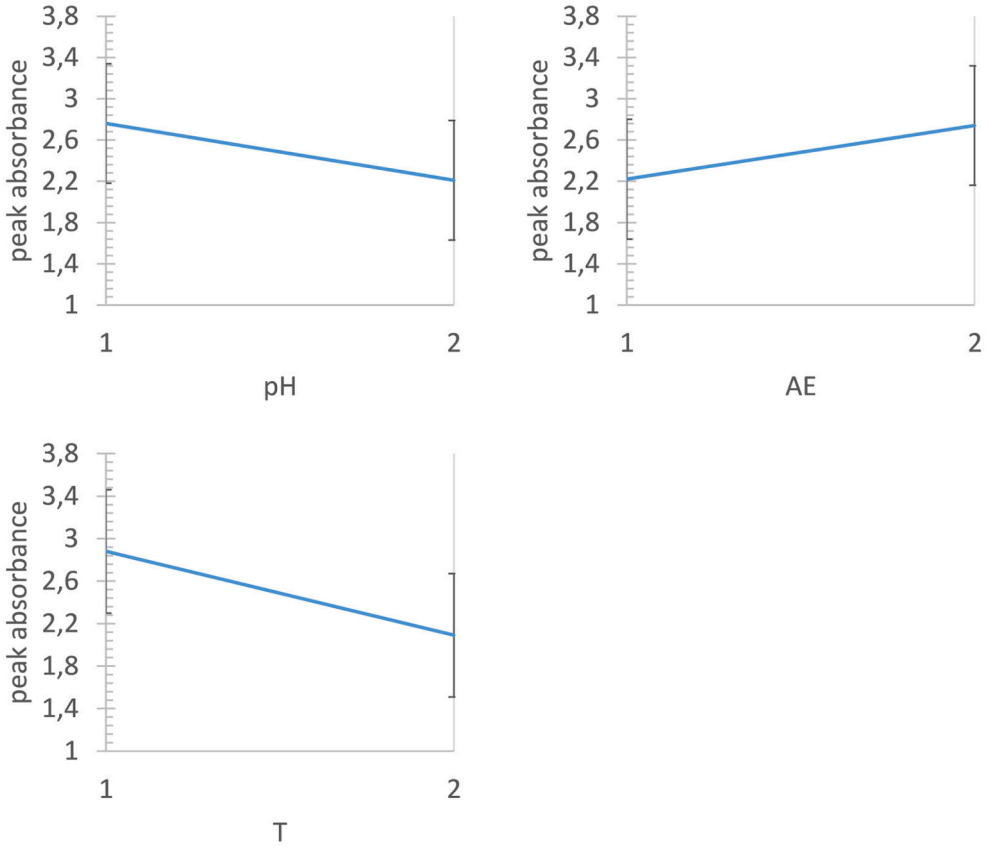

Fig. 8. Variation of the height of the absorbance of peak 386 nm with the synthesis parameters.

selected experimental run (shown in Table 5) with specific synthesis parameters values were characterized.

Fig. 9 compares the UV–Vis absorption spectra of confirmation run (Max 565), run 5 (Min 386) and run 7 (Max 565/ Min 386). Comparing to the confirmation run, the UV–Vis spectra for run 5 shows one main SPR peak at around 565 nm, suggesting the existence of essentially Cu phase microparticles. The broadness and the blue shift (from 583 nm to 565 nm) of the absorption peak probably stems from the wide size distribution of microparticles and a decrease in the mean particle size. Compared with the confirmation run settings, the differences are the higher solution temperature and the lower extract amount (AE). The UV–Vis spectra for run 7 shows two absorbance bands at 386 nm and at 530 nm, the presence of these two peaks indicating the coexistence of both Cu_2O and Cu, quite similar to what is observed in the confirmation run. There is also a reduction in the height of the two peaks which might be related to the lower amount and/or the aggregation of the different types of microparticles produced. Additionally, in the second broad peak, there was a blue shift (from 583 nm to 530 nm), which might indicate a decrease in the mean microparticle size. Compared with the confirmation run settings, the only difference is the higher solution temperature.

Fig. 10 shows the XRD patterns of samples from confirmation run, run 5 and run 7. Sample from run 5 shows the three main characteristic diffraction peaks of Cu particles, and a small peak at 29.87° which is assigned to (1 0 0) plane of Cu_2O. Run 5 shows Cu phase predominantly. Analysis of the ratio of Cu and Cu_2O determined from TOPAS software was 69% and 31%, respectively. The higher solution temperature and the decrease in the extract amount (AE) proved to be effective in reducing the synthesis of microparticles of oxidized Cu phase (from 83% to 31%). Run 7 shows diffraction peaks at 43.46°, 50.36° and 74.66° which are assigned to (1 1 1), (2 0 0), and (2 2 0) planes of face-centered cubic (fcc) crystal structure of Cu particles and diffraction peaks at 36.47°, 62.27° and 74.30° assigned to (1 1 1), (2 0 0), (2 2 0), (3 1 1) planes which corresponds to face-centered cubic (fcc) crystal structure of Cu_2O. The comparison between the XRD patterns of confirmation run and run 7 reveals very similar patterns, both samples

comprise mixed of both Cu and Cu_2O microparticles. The ratio of Cu and Cu_2O estimated using TOPAS software was 17% and 83% for the confirmation run and was 16% and 84% for run 7, a slight decrease on Cu particles amount. The only different between the synthesis conditions of these two runs is the synthesis temperature. From the XRD patterns the temperature alone had no significant effect on the Cu:Cu_2O ratio.

Fig. 11 shows the morphologies and EDS images of green synthesized copper microparticles from confirmation run, run 5 and run 7. Based on the obtained SEM images (Fig. 11a, c and e) it is observed a large quantity of green synthesized copper microparticles with spherical

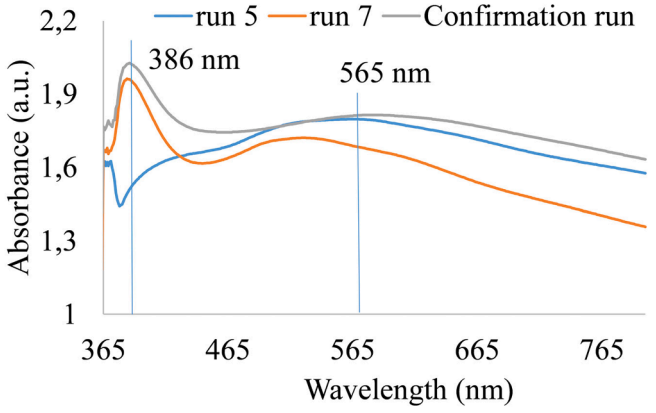

Fig. 9. UV–Vis absorption spectrum of microparticles produced from confirmation run, run 5 and run 7.

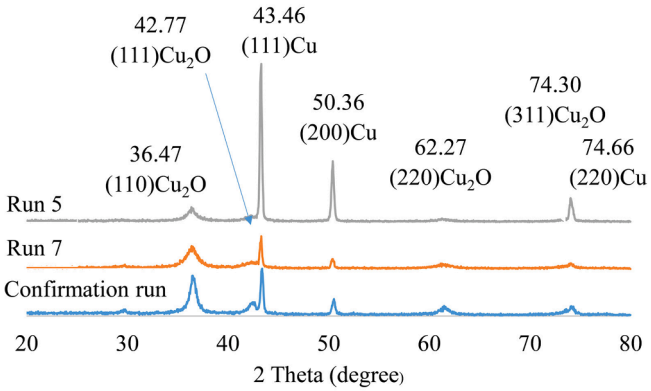

Fig. 10. XRD diffractogram of microparticles synthesized by CS extract from confirmation run, run 5 and run 7.

morphology for each experimental run, and the size of the nanoparticles are between 364 and 1125 nm, 324–711 nm and 385–738 nm for confirmation run, run 5 and run 7, respectively. Of all the runs, the confirmation run proved to have the widest size distribution of microparticles, which is consistent with UV–Vis analysis that showed the broadest peak at around 583 nm. Also, run 5 had the smaller mean particle size that might be related to the Cu phase of microparticles being predominant.

As seen in Fig. 11b, d and f, the elemental content of the produced microparticles was assessed using EDS analysis. The microparticles are composed of Cu along with O and C elements, as the main elements. The presence of Cu, the main element, confirms the formation of Cu microparticles. The O element, being mainly from the oxidation of copper particles [52], at 3.1%, 11.1% and 13.5% is present in run 5, run 7 and confirmation run. Run 5 has the least amount of O element proving to be the sample with the least oxidation of Cu microparticles.

Table 6 resumes the characterization of the produced copper particles for the different objectives envisaged.

As discussed, the pH of 12, the amount of CS extract of 4 mL, the copper salt precursor of 50 mM, and the temperature 90℃ and 1 h reaction are the optimum set of reaction conditions for the lowest absorbance peak at 386 nm (run 5), which led to the lowest amount of Cu_2O microparticles and consequently the highest amount of Cu microparticles (pure Cu phase). The ratio of Cu/Cu_2O was 69/31 wt% (run 5) instead of 17/83 wt% (confirmation run). Also, the confirmation run and run 7 give identical ratio of Cu/Cu_2O, the latter with less amount and with smaller particlés size. It may be concluded that the simultaneous increment of the reaction yield and the decrement of Cu particles oxidation is rendered difficult (with the current synthesis set-up).

Fig. 12 depicts schematically the influence of the more representative green synthesis parameters on the production of Cu/Cu_2O microparticles and on the minimization Cu particles oxidation. This influence can described as follows:

a) increasing pH (+pH) produces higher number of mixed Cu/Cu_2O microparticles with less Cu_2O particles in the mixture (increases peak at 565 nm, decreases peak at 386 nm);
b) increasing T (+T) produces less number of mixed Cu/Cu_2O microparticles with less Cu_2O microparticles, but particles have larger size (decreases peak at 565 nm, decreases peak at 386 nm);
c) increasing AE (+AE) produces higher number of mixed Cu/Cu_2O microparticles with high Cu_2O particles in the mixture (increases peak at 565 nm, increases peak at 386 nm).

3.5. Electrical resistivity measurement

Microparticles of confirmation run and of run 5 were used to prepare powder discs for electrical resistance measurements. The microparticles

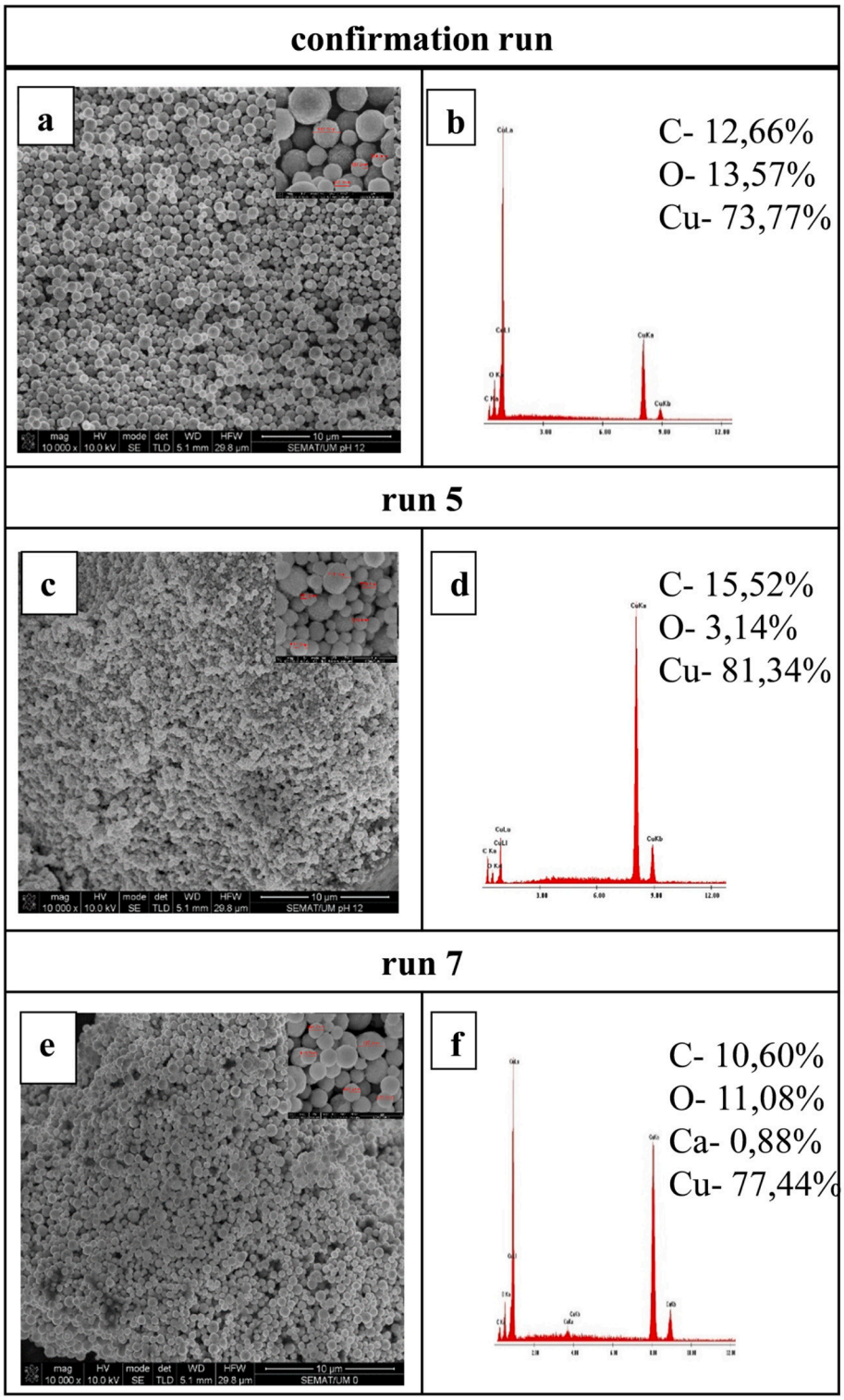

Fig. 11. SEM images of copper microparticles synthesized by CS extract, (a) confirmation run, (c) run 5 and (e) run 7 and EDS spectrum of copper nanoparticles synthesized by CS extract, (b) confirmation run, (d) run 5 and (f) run 7.

powders were pressureless sintering at 180 ℃ under N_2 atmosphere for 60 min prior to disc preparation. The electrical resistivity of confirmation run comprising 17% of copper microparticles (Cu) and 83% of copper oxide (Cu_2O) and of run 5 comprising 69% of copper microparticles (Cu) and 31% of copper oxide (Cu_2O) was of 4.99 Ω.cm and of 1.52×10^{-3} Ω.cm, respectively. Due to the fact that pure Cu_2O has reported resistivity measurements of 10 Ω.cm [56,57], it was expected that our Cu_2O rich sample (confirmation run) would present slight lower electrical resistivity values, as occurred. The electrical resistivity of run 5 is nearly 3 magnitudes less than those of the confirmation run, which should be attributed to the higher amount of pure copper (Cu) in the mixture. This result is a clear combination of metal and semiconductor characteristics of the produced particles. Pure Cu films produced by physical sputtering deposition have reported electrical resistivity values of 10^{-4} Ω.cm [56]. The low electrical resistivity of the green produced copper particles make them suitable for sensors and circuitry

Table 6
Resume of the characterization of synthetized Cu microparticles.

Objective:	UV–VIS	XRD (ratioCu/Cu_2O %)	SEM(particles size nm)	EDS(C, O, Cu amount %)	
Max peak 565 (Cu NP), confirmation run	386 nm and 560–585 nm peaks; Wide particle size distribution	17/83	364–1125	12.7/13.6/73.8	• Highest yield • Widest particle distribution • Oxidized Cu
Min peak 386 (Cu_2O NP), Run 5	No 386 nm peak, but blue shift 583 to 565 nm peak; lower mean particle size	69/31	324–711Smaller particle size	15.5/3.1/81,3	• Smallest particle size • Smallest oxidation of Cu
Max 565 and Min peak 386, Run 7	386 nm and 530 nm peaks; blue shift 583 to 530 nm peakLess amount of particles	18/84	385–738	10.6/11.1/77.4	• Lowest yield • Oxidized Cu

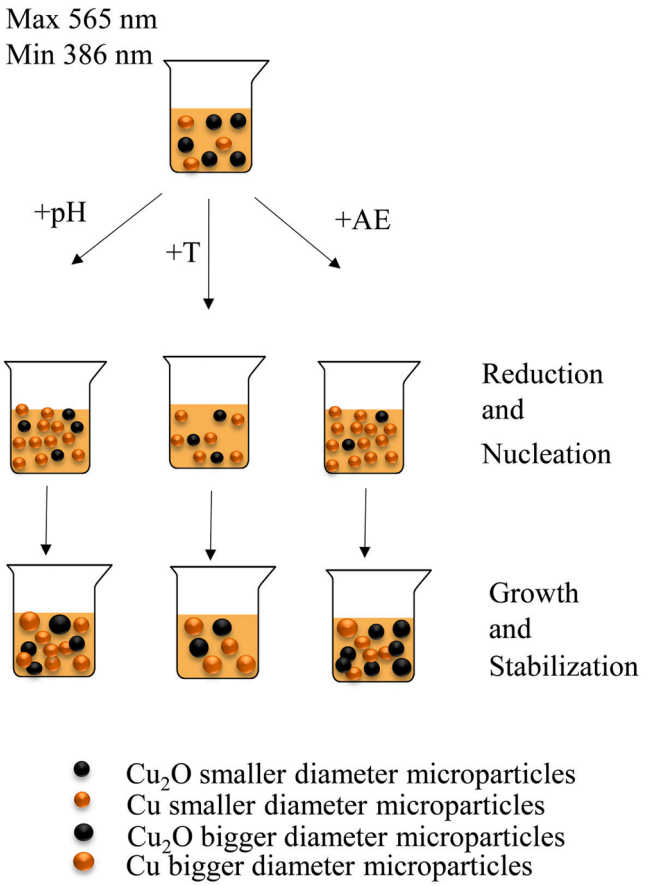

Fig. 12. Representative scheme of the green synthesis of Cu /Cu_2O microparticles with synthesis parameters variation. (For interpretation of the references to colour in this figure legend, the reader is referred to the web version of this article.)

components, as required in printed electronics applications.

4. Conclusions

Cu/Cu_2O microparticles were produced by green synthesis using artichoke (*Cynara scolymus L.*) plant extract, this being clean, non-toxic and environmentally friendly method. A design od experiments was applied for the optimization of green synthesis conditions for maximum yield production of Cu/Cu_2O microparticles and reduced oxidation of Cu microparticles.

Results showed the optimum set of synthesis parameters for higher yield production: 5 mL of CS extract, 50 mM of $Cu(NO_3)_2{\cdot}3H_2O$, pH of 12, and temperature of 80℃. The UV–Vis results confirmed the maximization of yield production. A maximum of 4.5 mg/mL of Cu/Cu_2O microparticles was synthesized. The ratio of Cu/Cu_2O was 17/83 (wt %) determined by XRD. Spherical particles of 364–1225 nm were observed by SEM. The electrical resistivity of the mixture Cu/Cu_2O (17/83 wt%) was 4.99 Ω.cm, the high value revealing an excessive amount of Cu oxide. Optimum synthesis parameters for minimization of Cu_2O phase microparticles were: 4 mL of CS extract, 50 mM of copper salt, pH of 12, and temperature of 90℃. UV–Vis and XRD confirmed the minimization of Cu_2O phase over Cu/Cu_2O mixture, the ratio of Cu/Cu_2O was 69/31 (wt %). Spherical particles of 324–711 nm were observed by SEM. The electrical resistivity tests (after pressureless sintering at 180℃ for 60 min) confirmed the resistivity of Cu/Cu_2O (69/31 wt%) was 1.52×10^{-3} Ω.cm, this lower value validating the proposed approach. The use of the Taguchi method allowed to conclude that the simultaneous increasing of the reaction yield and the decrement of less oxidized Cu particles is rendered difficult with the adopted synthesis approach.

This work demonstrates a simple and effective design method to optimize green synthesis of copper microparticles to obtain maximization of the yield production, and, for the first time, to reduce the extent of the oxidation of copper particles that renders into an improvement of the electrical properties of the microparticles. The Taguchi method associated with the green synthesis of nanoparticles is a reliable, cost-effective and environmentally friendly process that can be used in an industrial and more massive scale.

Declaration of Competing Interest

The authors declare that they have no known competing financial interests or personal relationships that could have appeared to influence the work reported in this paper.

Acknowledgments

This work was supported by the North Portugal Regional Operational Programme (NORTE 2020), under the Portugal 2020 Partnership Agreements [project TSSiPRO - TECHNOLOGIES FOR SUSTAINABLE AND SMART INNOVATIVE PRODUCTS, N° NORTE-01-0145-FEDER-000015].

Data Availability

The raw/processed data required to reproduce these findings cannot be shared at this time due to technical or time limitations.

References

[1] A.P. LaGrow, M.R. Ward, D.C. Lloyd, P.L. Gai, E.D. Boyes, Visualizing the Cu/Cu 2 O Interface Transition in Nanoparticles with Environmental Scanning Transmission Electron Microscopy, J. Am. Chem. Soc. 139 (1) (2017) 179–185.
[2] X. Dai, W. Xu, T. Zhang, T. Wang, Self-Reducible Cu Nanoparticles for Conductive Inks, Ind. Eng. Chem. Res. 57 (7) (2018) 2508–2516.

[3] D. Han, X. Li, X. Zhao, J. Feng, Y. Qian, Hydrothermal Synthesis of Copper Nanowires as Advanced Conductive Agents for Lithium Ion Batteries, j nanosci nanotechnol 15 (9) (2015) 7177–7180.
[4] Y. An, H. Fei, G. Zeng, X. Xu, L. Ci, B. Xi, S. Xiong, J. Feng, Y. Qian, Vacuum distillation derived 3D porous current collector for stable lithium–metal batteries, Nano Energy 47 (2018) 503–511.
[5] P. Shen, Y. Liu, Y. Long, L. Shen, B. Kang, High-Performance Polymer Solar Cells Enabled by Copper Nanoparticles-Induced Plasmon Resonance Enhancement, J. Phys. Chem. C 120 (16) (2016) 8900–8906.
[6] Z. Qing, A. Bai, S. Xing, Z. Zou, X. He, K. Wang, R. Yang, Progress in biosensor based on DNA-templated copper nanoparticles, Biosens. Bioelectron. 137 (2019) 96–109.
[7] A.I. Ayesh, A.A. Alyafei, R.S. Anjum, R.M. Mohamed, M.B. Abuharb, B. Salah, M. El-Muraikhi, Production of sensitive gas sensors using CuO/SnO2 nanoparticles, Appl. Phys. A 125 (8) (2019), https://doi.org/10.1007/s00339-019-2856-6.
[8] G. Karim-Nezhad, Z. Khorablou, P.S. Dorraji, A promising electrochemical sensing platform based on copper nanoparticles-decorated polymer in carbon nanotube electrode for monitoring methimazole, J IRAN CHEM SOC 15 (4) (2018) 905–913.
[9] M.B. Gawande, A. Goswami, F.-X. Felpin, T. Asefa, X. Huang, R. Silva, X. Zou, R. Zboril, R.S. Varma, Cu and Cu-Based Nanoparticles: Synthesis and Applications in Catalysis, Chem. Rev. 116 (6) (2016) 3722–3811.
[10] M.H. Ravari, A. Sarrafi, M. Tahmooresi, Synthesizing and characterizing the mixed Al,Cu-pillared and copper doped Al-pillared bentonite for electrocatalytic reduction of CO2, S. Afr. J. Chem. Eng. 31 (2020) 1–6.
[11] J. Peternela M.F. Silva M.F. Vieira R. Bergamasco A.M.S. Vieira Synthesis and Impregnation of Copper Oxide Nanoparticles on Activated Carbon through Green Synthesis for Water Pollutant Removal Mat. Res. 21 1 10.1590/1980-5373-mr-2016-0460 http://www.scielo.br/scielo.php?script=sci_arttext&pid=S1516-14392018000100135&lng=en&tlng=en.
[12] G. Sánchez-Sanhueza D. Fuentes-Rodríguez H. Bello-Toledo Copper Nanoparticles as Potential Antimicrobial Agent in Disinfecting Root Canals: A Systematic Review Int. J. Odontostomat. 10 3 547 554 10.4067/S0718-381X2016000300024 http://www.scielo.cl/scielo.php?script=sci_arttext&pid=S0718-381X2016000300024&lng=en&nrm=iso&tlng=en.
[13] U. Bogdanović, V. Lazić, V. Vodnik, M. Budimir, Z. Marković, S. Dimitrijević, Copper nanoparticles with high antimicrobial activity, Mater. Lett. 128 (2014) 75–78.
[14] N. Pariona, A.I. Mtz-Enriquez, D. Sánchez-Rangel, G. Carrión, F. Paraguay-Delgado, G. Rosas-Saito, Green-synthesized copper nanoparticles as a potential antifungal against plant pathogens, RSC Adv. 9 (33) (2019) 18835–18843.
[15] Halevas E and Pantazaki A 2018 Copper Nanoparticles as Therapeutic Anticancer Agents 119.
[16] Q. Fu, M. Stein, W. Li, J. Zheng, F.E. Kruis, Conductive films prepared from inks based on copper nanoparticles synthesized by transferred arc discharge, Nanotechnology 31 (2) (2020) 025302, https://doi.org/10.1088/1361-6528/ab4524.
[17] C.-Y. Tsai, W.-C. Chang, G.-L. Chen, C.-H. Chung, J.-X. Liang, W.-Y. Ma, T.-N. Yang, A Study of the Preparation and Properties of Antioxidative Copper Inks with High Electrical Conductivity, Nanoscale Res Lett 10 (1) (2015), https://doi.org/10.1186/s11671-015-1069-y.
[18] P. Lignier, R. Bellabarba, R.P. Tooze, Scalable strategies for the synthesis of well-defined copper metal and oxidenanocrystals, Chem. Soc. Rev. 41 (5) (2012) 1708–1720.
[19] H. Khanehzaei, M. Ahmad, S. Kamyar, Z. Ajdari, Synthesis and Characterization of Cu@Cu 2 O Core Shell Nanoparticles Prepared in Seaweed Kappaphycus alvarezii, Media vol 9 (2014).
[20] V.V. Makarov A.J. Love O.V. Sinitsyna S.S. Makarova I.V. Yaminsky M.E. Taliansky N.O. Kalinina "Green" Nanotechnologies: Synthesis of Metal Nanoparticles Using Plants Acta Naturae 6 1 35 44 10.32607/20758251-2014-6-1-35-44 http://actanaturae.ru/2075-8251/article/view/10554.
[21] T. Shankar, P. Karthiga, K. Swarnalatha, K. Rajkumar, Green synthesis of silver nanoparticles using Capsicum frutescence and its intensified activity against E. coli, Resour.-Effic. Technol. 3 (3) (2017) 303–308.
[22] S. Ganguly, S. Mondal, P. Das, P. Bhawal, T.K. Das, M. Bose, S. Choudhary, S. Gangopadhyay, A.K. Das, N.C. Das, Natural saponin stabilized nano-catalyst as efficient dye-degradation catalyst, Nano-Structures & Nano-Objects 16 (2018) 86–95.
[23] Shanmugam R, KANNAN C and Gurusamy A 2012 Green synthesis of silver nanoparticles using marine brown Algae turbinaria conoides and its antibacterial activity vol 3.
[24] Lakhi Chetia, Debabrat Kalita, Gazi A. Ahmed, Synthesis of Ag nanoparticles using diatom cells for ammonia sensing, Sens. Bio-Sens. Res. 16 (2017) 55–61.
[25] C. Ankit, A. Singh, M. Sharma, Biological Synthesis of Nanoparticles Using Bacteria and Their Applications vol 4 (2014).
[26] F. Niknejad, M. Nabili, R. Daie Ghazvini, M. Moazeni, Green synthesis of silver nanoparticles: Advantages of the yeast Saccharomyces cerevisiae model *Curr*, Med. Mycol. 1 (2015) 17–24.
[27] M. Sastry, A. Ahmad, M. Islam Khan, R. Kumar, Biosynthesis of metal nanoparticles using fungi and actinomycete vol 85 (2003).
[28] Waleed A. El-Said, Hyeon-Yeol Cho, Cheol-Heon Yea, Jeong-Woo Choi, Synthesis of Metal Nanoparticles Inside Living Human Cells Based on the Intracellular Formation Process, Adv. Mater. 26 (6) (2014) 910–918.
[29] H. Lee, J. Yong Song, B.S. Kim, Biological synthesis of copper nanoparticles using Magnolia kobus leaf extract and their antibacterial activity vol 88 (2013).
[30] P Padma Syed Banu S Kumari Studies on Green Synthesis of Copper Nanoparticles Using Punica granatum ARRB 23 1 1 10 10.9734/ARRB 10.9734/ARRB/2018/38894 http://www.sciencedomain.org/journal/32 http://www.sciencedomain.org/abstract/22925.
[31] S. Ramasamy, M. Selvam, Green synthesis of copper nanoparticles from Hibicus rosasinensis and their antimicrobial, antioxidant activities vol 6 (2015).
[32] I.-M. Chung, A. Abdul Rahuman, S. Marimuthu, A.V. Kirthi, K. Anbarasan, P. Padmini, G. Rajakumar, Green synthesis of copper nanoparticles using Eclipta prostrata leaves extract and their antioxidant and cytotoxic activities, Exp Ther. Med. 14 (2017) 18–24.
[33] Saranyaadevi K, Subha V, R S E R and Renganathan S 2014 Synthesis and Characterization of Copper Nanoparticle using Capparis Zeylanicaleaf Extract vol 6.
[34] H. Raja Naika, K. Lingaraju, K. Manjunath, Danith Kumar, G. Nagaraju, D. Suresh, H. Nagabhushana, Green synthesis of CuO nanoparticles using Gloriosa superba L. extract and their antibacterial activity, Journal of Taibah University for Science 9 (1) (2015) 7–12.
[35] G. Princy, B.N. Srri, U. Poonguzhali, N. Gandhi, S. Renganathan, A review on green synthesis of silver nanoparticles *Asian*, J. Pharm. Clin. Res. 6 (2013) 8–12.
[36] Jiménez-Moreno Cimminelli Volpe Ansó Esparza Mármol Rodríguez-Yoldi Ancín-Azpilicueta Phenolic Composition of Artichoke Waste and its Antioxidant Capacity on Differentiated Caco-2 Cells Nutrients 11 8 1723 10.3390/nu11081723 https://www.mdpi.com/2072-6643/11/8/1723.
[37] A. Gaafar, A. Salama, Z,, Phenolic Compounds from Artichoke (Cynara scolymus L.) By- products and their Antimicrobial Activities, J. Biol. Agric. Healthc. 3 (2013) 1–7.
[38] FAOSTAT, Crops, Artichokes Food Agric. Organ, United Nations, 2016.
[39] Sandra Sampaio Júlio C Viana Production of silver nanoparticles by green synthesis using artichoke (Cynara scolymus L.) aqueous extract and measurement of their electrical conductivity Adv. Nat. Sci: Nanosci. Nanotechnol. 9 4 045002 10.1088/2043-6254/aae987 https://iopscience:iop.org/article/10.1088/2043-6254/aae987.
[40] A. Dar, N. Anuradha, An application of Taguchi L9 method in black scholes model for European call option, Int. J. Entrep. 22 (2018).
[41] Sapana S. Madan, Kailas L. Wasewar, Optimization for benzeneacetic acid removal from aqueous solution using CaO 2 nanoparticles based on Taguchi method, J. Appl. Res. Technol. 15 (4) (2017) 332–339.
[42] K. Jagajjanani Rao, Santanu Paria, Aegle marmelos Leaf Extract and Plant Surfactants Mediated Green Synthesis of Au and Ag Nanoparticles by Optimizing Process Parameters Using Taguchi Method, ACS Sustainable Chem. Eng. 3 (3) (2015) 483–491.
[43] Zahra Aghajani Kalaki Raheleh SafaeiJavan Hossein Faraji Procedure optimisation for green synthesis of silver nanoparticles by Taguchi method 13 4 2018 558 561 https://digital-library.theiet.org/content/journals/10.1049/mnl.2017.0308.
[44] EL-Moslamy S H, Elkady M F, Rezk A H and Abdel-Fattah Y R 2017 Applying Taguchi design and large-scale strategy for mycosynthesis of nano-silver from endophytic Trichoderma harzianum SYA.F4 and its application against phytopathogens Sci. Rep. 7 45297.
[45] Shahira H. EL-Moslamy, Marwa F. Elkady, Ahmed H. Rezk, Yasser R. Abdel-Fattah, Applying Taguchi design and large-scale strategy for mycosynthesis of nano-silver from endophytic Trichoderma harzianum SYA.F4 and its application against phytopathogens, Sci Rep 7 (1) (2017), https://doi.org/10.1038/srep45297.
[46] How-Ji Chen Sheng-Nan Chang Chao-Wei Tang Application of the Taguchi Method for Optimizing the Process Parameters of Producing Lightweight Aggregates by Incorporating Tile Grinding Sludge with Reservoir Sediments Materials 10 11 1294 10.3390/ma10111294 http://www.mdpi.com/1996-1944/10/11/1294.
[47] Jagpreet Singh, Tanushree Dutta, Ki-Hyun Kim, Mohit Rawat, Pallabi Samddar, Pawan Kumar, 'Green' synthesis of metals and their oxide nanoparticles: applications for environmental remediation, J Nanobiotechnol 16 (1) (2018), https://doi.org/10.1186/s12951-018-0408-4.
[48] Ragaa A. Hamouda, Mervat H. Hussein, Rasha A. Abo-elmagd, Salwa S. Bawazir, Synthesis and biological characterization of silver nanoparticles derived from the cyanobacterium Oscillatoria limnetica, Sci Rep 9 (1) (2019), https://doi.org/10.1038/s41598-019-49444-y.
[49] Clément Barrière, Kilian Piettre, Virginie Latour, Olivier Margeat, Cédric-Olivier Turrin, Bruno Chaudret, Pierre Fau, Ligand effects on the air stability of coppernanoparticles obtained from organometallic synthesis, J. Mater. Chem. 22 (5) (2012) 2279–2285.
[50] Thirugnanasambandan T and Alagar M 2010 X-Ray Diffraction Studies of Copper Nanopowder Arch Phys Res 1.
[51] Liangbin Xiong, Huaqing Xiao, Shunsheng Chen, Zhihong Chen, Xunong Yi, Sheng Wen, Genwen Zheng, Yaoming Ding, Huaqing Yu, Fast and simplified synthesis of cuprous oxide nanoparticles: annealing studies and photocatalytic activity, RSC Adv. 4 (107) (2014) 62115–62122.
[52] Noemi Jardón-Maximino, Marissa Pérez-Alvarez, Rubén Sierra-Ávila, Carlos Alberto Ávila-Orta, Enrique Jiménez-Regalado, Angélica Mara Bello, Pablo González-Morones, Gregorio Cadenas-Pliego, Oxidation of Copper Nanoparticles Protected with Different Coatings and Stored under Ambient Conditions, Journal of Nanomaterials 2018 (2018) 1–8.
[53] Jagdeep Singh, Amarjit Singh Dhaliwal, Novel Green Synthesis and Characterization of the Antioxidant Activity of Silver Nanoparticles Prepared from Nepeta leucophylla Root Extract, Anal. Lett. 52 (2) (2019) 213–230.
[54] Luca Valgimigli, Andrea Baschieri, Riccardo Amorati, Antioxidant activity of nanomaterials, J. Mater. Chem. B 6 (14) (2018) 2036–2051.
[55] Prithviraj Chakraborty, Surajit Dey, Versha Parcha, Shiv Sankar Bhattacharya, Amitava Ghosh, Design Expert Supported Mathematical Optimization and

Predictability Study of Buccoadhesive Pharmaceutical Wafers of Loratadine, Biomed Res. Int. 2013 (2013) 1–12.

[56] Su J, Liu Y, Jiang M and Zhu X 2014 Oxidation of copper during physical sputtering deposition: mechanism, avoidance and utilization.

[57] A. Ogwu, T. Darma, E. Bouquerel, Electrical resistivity of copper oxide thin films prepared by reactive magnetron sputtering, J. Achiev. Mater. Manuf Eng. (2007) 24.